Applied Physics Letters

RESEARCH ARTICLE | FEBRUARY 20 2024

Highly tailorable thermomechanical properties of nanograined silicon: Importance of grain size and grain anisotropy

Jiahui Cao ; Han Wang ; Laia Ferrer-Argemi ; Penghui Cao ; Jaeho Lee

Appl. Phys. Lett. 124, 082201 (2024)
https://doi.org/10.1063/5.0185911

AIP Publishing

Applied Physics Letters ARTICLE pubs.aip.org/aip/apl

Highly tailorable thermomechanical properties of nanograined silicon: Importance of grain size and grain anisotropy

Cite as: Appl. Phys. Lett. **124**, 082201 (2024); doi: 10.1063/5.0185911
Submitted: 2 November 2023 · Accepted: 28 January 2024 ·
Published Online: 20 February 2024

Jiahui Cao, Han Wang, Laia Ferrer-Argemi, Penghui Cao, and Jaeho Lee[a)]

AFFILIATIONS

Department of Mechanical and Aerospace Engineering, University of California, Irvine, California 92697, USA

[a)]Author to whom correspondence should be addressed: jaeholee@uci.edu

ABSTRACT

Nanocrystalline silicon can have unique thermal transport and mechanical properties governed by its constituent grain microstructure. Here, we use phonon ray-tracing and molecular dynamics simulations to demonstrate the largely tunable thermomechanical behaviors with varying grain sizes (a_0) and aspect ratios (ξ). Our work shows that, by selectively increasing the grain size along the heat transfer direction while keeping the grain area constant, the in-plane lattice thermal conductivity (k_x) increases more significantly than the cross-plane lattice thermal conductivity (k_y) due to anisotropic phonon–grain boundary scattering. While k_x generally increases with increasing ξ, a critical value exists for ξ at which k_x reaches its maximum. Beyond this transition point, further increases in ξ result in a decrease in k_x due to substantial scattering of low-frequency phonons with anisotropic grain boundaries. Moreover, we observe reductions in the elastic and shear modulus with decreasing grain size, and this lattice softening leads to significant reductions in phonon group velocity and thermal conductivity. By considering both thermal and mechanical size effects, we identify two distinct regimes of thermal transport, in which anisotropic phonon–grain boundary scattering becomes more appreciable at low temperatures and lattice softening becomes more pronounced at high temperatures. Through phonon spectral analysis, we attribute the significant thermal conductivity anisotropy in nanograined silicon to grain boundary scattering of low-frequency phonons and the softening-driven thermal conductivity reduction to Umklapp scattering of high-frequency phonons. These findings offer insights into the manipulation of thermomechanical properties of nanocrystalline silicon via microstructure engineering, carrying profound implications for the development of future nanomaterials.

Nanostructuring has become a powerful approach to reducing silicon's intrinsic high thermal conductivity. Experimental investigations on polysilicon[1,2] and Si nanoporous structures[3–6] have demonstrated significant reductions in thermal conductivity due to phonon ballistic thermal transport[5] and thermally dead volume.[6] Unlike nanowires,[7–9] nanomeshes,[10,11] and nanoribbons,[6,12] where phonon-boundary scatterings strongly depend on simple geometric parameters, such as diameters, our understanding of phonon–grain boundary scattering, particularly its frequency-dependent characteristics, remains incomplete. Early studies[13–15] used the average grain size as a mean free path (MFP) or a gray (frequency-independent) model; however, experimental data[1,16] and atomistic simulation[17] revealed a sharp decrease in phonon transmission probability at higher frequencies.[18] Another crucial factor in these studies is the treatment of phonons crossing the grain boundary interfaces. While most theoretical studies on polysilicon have relied on Monte Carlo ray-tracing (MCRT) simulations with the assumption of diffuse reflection or transmission at grain boundaries,[2,19] Hua and Minnich[20] defined a specularity parameter for both reflected and transmitted phonons, and Chakraborty *et al.*[21] considered a completely specular transmission. Since only Hua and Minnich validated their modeling with one experimental dataset, further investigation is needed to compare the different phonon treatments. Moreover, MCRT simulations are computationally expensive and usually contain geometric scales smaller than the average mean free path;[22] therefore, there has been no research on the impacts of grain boundary orientation and anisotropy. Nevertheless, recent developments in nanocomposite materials, such as nanograined diamond films with triangular hierarchical grains and nanowire-based pallets with greatly elongated grains,[23,24] have motivated us to develop analytical and numerical models to study the thermomechanical properties inherent in these intriguing grain structures.

While the reduction of thermal conductivity in nanostructures is often attributed to a reduced mean free path arising from boundary

scattering, reducing the grain size to the nanoscale can significantly impact both mechanical and thermal transport behaviors. In general, the strength of polycrystalline metals increases as grain size decreases,[25] peaking around 20–30 nm.[26–28] Beyond this critical size, materials exhibit softening due to a transition from dislocation-mediated plasticity to grain-boundary-mediated deformation.[29] Studies have also demonstrated the dependence of microhardness and elastic modulus on the grain size of nanocrystalline silicon.[30–32] Molecular dynamic (MD) simulations have further underscored the role of grain boundaries in polysilicon, highlighting their potential as preferential sites for high-pressure phase transformations.[33] Nevertheless, the elastic behavior of a material is closely linked to its thermal transport properties. Studies have shown that lattice softening leads to an additional reduction in thermal conductivity, stemming from a decreased phonon group velocity.[34,35] In principle, the change in the speed of sound ($V_s = \sqrt{E/\rho}$, where E is the Young's modulus and ρ is the density), directly proportional to $\sqrt{E}$ in the continuum limit, can serve as an estimate for the change in average phonon group velocity[35] (i.e., $\bar{v}_g^3 \propto V_s^3 \propto E^{3/2}$; see supplementary material Note 1). In the case of nanocrystalline silicon, the lattice stiffness, and thus the thermal conductivity, can be tailored by controlling the average grain size of nanoparticles that undergo consolidation via spark plasma sintering (SPS).[36] Moreover, tuning the lattice stiffness can exert a more significant impact on lattice thermal conductivity than micro-/nanostructural scattering, especially at high temperatures.[35]

In this study, we use 2D heat-flux-driven Monte Carlo ray tracing to investigate phonon–grain boundary scattering in nanograined silicon. We first validate our semi-numerical model against experimental data.[1] We then examine the impact of grain anisotropy on phonon–grain boundary scattering mean free paths (Λ_{GB}) in nanograined silicon with homogenous grain structures and evaluate their contribution to temperature-dependent thermal conductivity and thermal anisotropy. On the other hand, we perform 3D atomistic simulations, using the large-scale atomic/molecular massively parallel simulator (LAMMPS), to study the mechanical behaviors of nanograined silicon with heterogeneous grain structures resembling those in natural and synthetic materials. We investigate the mechanical size effect and the influence of grain anisotropy on elastic and shear moduli and determine the critical grain size at which lattice softening occurs (i.e., when the elastic properties deviate from the bulk properties). Considering the weak grain boundary activities in the micro-elastic stage and that both homogenous grain structures in MCRT simulations and heterogeneous grain structures in MD simulations (see Fig. 1) share the same degree of gain anisotropy, we reasonably assume that grain heterogeneity has a negligible impact on elastic and shear moduli. Therefore, by incorporating the simulated moduli and their relationship to the average speed of sound, we modify the Born–von Karman (BvK) dispersion relation for bulk silicon to account for the effect of lattice softening on the thermal conductivity of nanograined silicon. This work advances our understanding of thermal transport across various temperature and size regimes and provides a valuable guide for grain structure engineering.

The lattice thermal conductivity can be calculated using the kinetic theory,

$$k_L = \frac{1}{3}\sum_{pol.}\int C_\nu v_g \Lambda_{\text{eff}}\, d\omega, \tag{1}$$

where ω is the phonon angular frequency, C_ν is the spectral volumetric heat capacity, v_g is the phonon group velocity, Λ_{eff} is the effective mean free path, and the summation runs over all phonon polarizations. We use the triply degenerate isotropic BvK sine-type dispersion[37] and Matthiessen's rule: $\Lambda_{\text{eff}}^{-1} = \Lambda_B^{-1} + \Lambda_I^{-1} + \Lambda_U^{-1}$ to combine boundary, impurity, and Umklapp scatterings, respectively [see supplementary material Note 2 for more details regarding the Boltzmann transport equation (BTE) model]. Although silicon's dispersion relations are not isotropic, studies[38,39] have shown that the Born von Karman (BvK) model, where the longitudinal acoustic (LA) and two transverse acoustic (TA) branches are lumped into one effective branch, adequately describes phonon transport in bulk and nanostructured silicon. Moreover, Λ_I and Λ_U have been well studied for silicon,[38–41] and the greatest challenge is in determining the mean free path for grain boundary scattering (Λ_{GB}). While there exist several

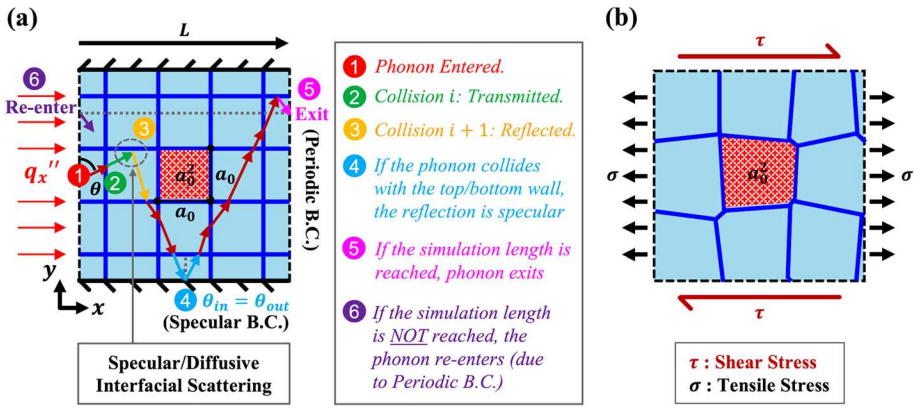

FIG. 1. Schematics of the simulated nanograined silicon geometry. (a) Ray-tracing simulation domain illustrating a possible phonon trajectory and various phonons interactions with grain boundaries and system domain boundaries (see supplementary material Note 3 for more details of the transmission algorithm). (b) Molecular dynamic simulation domain displaying the applied tensile and shear stresses. In the MD simulation domain, random grain boundary misalignments are introduced for mechanical stability at grain boundary junctions, resulting in a heterogeneous grain structure resembling those in natural and synthetic materials. This grain heterogeneity has little impact on the elastic and shear moduli due to weak grain boundary activities in the micro-elastic stage.[37] Therefore, MD simulations should yield similar results if a homogenous structure is simulated.

analytical and simulation models for Λ_{GB} of nanocrystalline silicon with uniform grain structure,[1,13,20] Λ_{GB} is generally unknown for anisotropic grain structures. To rigorously determine the frequency-dependent Λ_{GB} for these structures, we combine MCRT simulations with an atomistic correlation for grain boundary transmission.

One of the unique advantages of MCRT is its capability to account for multi-dimensional phonon-boundary scattering, enabling us to analyze the impact of anisotropic grain boundaries on Λ_{GB} and investigate thermal anisotropy in materials. Here, we choose 2D ray tracing simulation since we are interested in thermal transport in laterally confined systems, where boundary scattering phenomena on the top and bottom surface boundaries are less relevant compared to those along the heat transfer direction [see Fig. 1(a)]. While there is no fundamental difference between 2D and 3D ray tracing simulations, the 2D analysis significantly reduces the computational load (see supplementary material Note 3 for more details on the 2D vs 3D MCRT framework). Our group has used 2D MCRT simulations to evaluate Λ_B of nanoporous materials with various shapes and distributions,[42] as well as nanocomposite materials with these shapes being inclusions of metallic materials.[43] In this study, we use MCRT simulations to evaluate Λ_{GB} as a function of grain boundary transmission probability (τ_{GB}). For each grain structure, we computed Λ_{GB} for ten different τ_{GB} values and obtained a nonlinear fitting form in terms of τ_{GB},

$$\Lambda_{GB}(\tau_{GB}) = \frac{A_1 \tau_{GB}^{A_2}}{1 - \tau_{GB}}, \tag{2}$$

where A_1 and A_2 are two fitting parameters that depend on the grain size (a_0) and aspect ratio (ξ), respectively (see Table I for the fitting parameters for various grain structures; also see supplementary material Note 4 and Fig. S4 for the convergence and fitting of Λ_{GB}). We then combine this fitting function with a frequency-dependent atomistic expression for grain transmission probability[1,20] [Eq. (3)] to yield a frequency-dependent $\Lambda_{GB}(\omega)$,

$$\tau_{GB}(\omega) = \frac{1}{\gamma_{RT}\left(\frac{\omega}{\omega_0}\right) + 1}, \tag{3}$$

where $\gamma_{RT} = \frac{3}{4} \cdot \frac{1}{\alpha\beta}$ is a lumped fitting parameter comprised of an empirical constant α and a numerical constant β. The former accounts for grain boundary transmission or the grain boundary quality in a material.[1] In silicon materials, a native SiO_2 layer (typically around 1 nm thick[44]) usually forms on the outermost surface of each agglomerate when exposed to the atmosphere, resulting in oxidized grain boundaries. This leads to a smaller α or a larger γ_{RT}, and consequently, a lower thermal conductivity. The latter depends on the choice of dispersion relations[1] and is approximately 0.707. This frequency-dependent model is qualitatively consistent with atomistic Green's function calculations.[45,46] τ_{GB} approaches one as ω goes to zero, aligning with the expectation that long wavelength phonons remain unaffected by atomistic disorder at a grain boundary.[20] To validate our model, we compare $\Lambda_{GB}(\omega)$ obtained from MCRT simulations with the semi-empirical model from Wang *et al.*,[1] expressed as $\Lambda_{GB} = \alpha D_{avg}(\beta\omega_0/\omega)$, where D_{avg} is the average grain size/diameter and ω_0 is the cutoff frequency. The fitting yields a γ_{RT} value of 1.13 (see supplementary material Note 5 and Fig. S5.1), and the calculated thermal conductivities are consistent with the experimental data shown in Fig. 5(a).

TABLE I. Λ_{GB} fitting parameters and interfacial densities for various grain structures. The aspect ratio (ξ) characterizes the degree of grain anisotropy of the simulated unit cells; it is defined in such a way that the grain area, a_0^2, remains constant, where a_0 denotes the effective grain size. The interfacial density (ϕ) is calculated by dividing the perimeter of the grain by its area, $\phi = 2 \times [(a_0 \times \sqrt{\xi}) + (a_0/\sqrt{\xi})]/a_0^2$, and the interfacial density along the heat flux direction (ϕ_x) is defined as the reciprocal of the horizontal grain size, $\phi_x = 1/(a_0 \times \sqrt{\xi})$. The color code is consistent with that of Fig. 2 and Figs. 3(a) and 3(c).

ξ	A_1 (nm)	A_2	ϕ (μm^{-1})	ϕ_x (μm^{-1})	Configurations
256	48.3	0.388	321.3	0.6	$\xi > 1$
128	56.7	0.386	228.0	0.9	
64	63.4	0.382	162.5	1.3	
32	69.5	0.357	116.7	1.8	
16	74.7	0.442	85.0	2.5	
8	78.2	0.552	63.6	3.5	
4	79.7	0.781	50.0	5.0	$\xi = 1$
2	70.1	0.850	42.4	7.1	
1	57.7	0.885	40.0	10.0	
1/2	45.8	0.932	42.4	14.1	
1/4	34.7	0.978	50.0	20.0	
1/8	25.1	0.962	63.6	28.3	
1/16	18.2	0.988	85.0	40.0	$\xi < 1$
1/32	13.1	0.981	116.7	56.6	
1/64	9.3	0.992	162.5	80.0	
1/128	6.6	0.995	228.0	113.1	
1/256	4.8	1.000	321.3	160.0	

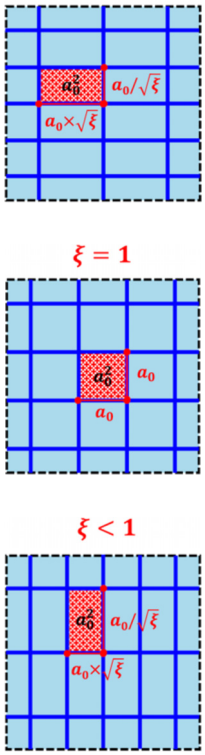

Extreme grain elongations or high grain aspect ratios in nanograined silicon can be achieved by utilizing nanowires as precursors for pallets, where alignment can be established through techniques such as flow[47] and magnetic alignments[48] or nanowire combing.[49] To investigate the impacts of grain anisotropy on Λ_{GB}, lattice thermal conductivity, and thermal anisotropy, we studied anisotropic grain structures with a fixed grain area of 10 000 nm^2 and varied ξ from 1/256 to 256. As shown in Figs. 2(a) and 2(b), Λ_{GB} monotonically increases with τ_{GB} and decreases with ω. This behavior confirms that long wavelength phonons (low frequency) are unaffected by atomistic disorder at a grain boundary.[20] While Λ_{GB} generally increases with ξ, the curves flatten for $\xi \geq 8$, resulting in an inverse trend at high τ_{GB} for these high-ξ structures. This inverse trend can be justified mathematically by a decrease in the fitting parameter, A_2, of Eq. (2). The inverse trend is also evident in Fig. 2(b), where Λ_{GB} at low frequency decreases as ξ exceeds 8. Figure 2(c) illustrates the relative contribution of each scattering mechanism over a wide temperature range. Clearly, Λ_{eff} is

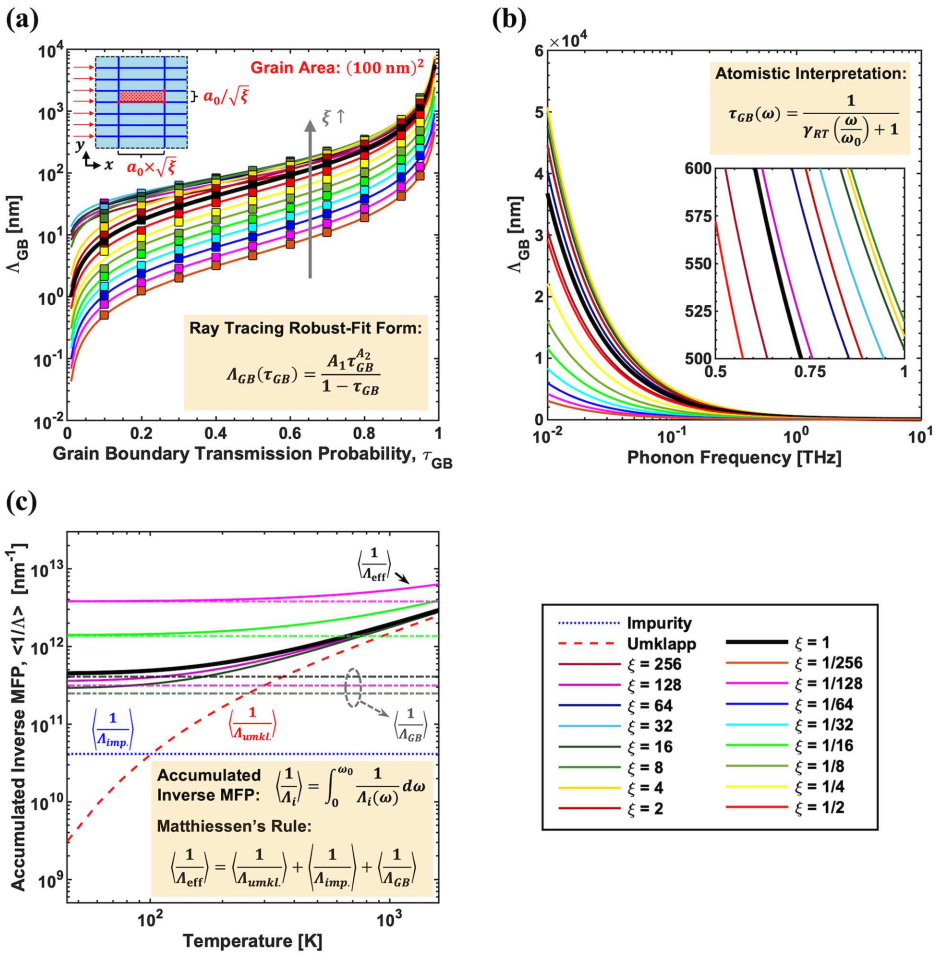

FIG. 2. Phonon mean free paths in nanograined silicon with a constant grain area of 10 000 nm^2. Λ_{GB} as a function of (a) grain boundary transmission probability, τ_{GB}, (b) phonon frequency, ω, and (c) accumulated inverse mean free paths, $\langle 1/\Lambda_i\rangle$, as a function of temperature. $\langle 1/\Lambda_i\rangle$ is computed by integrating $1/\Lambda_i(\omega)$ from 0 to ω_0 over the frequency, where the subscript i denotes the type of scattering mechanism. The solid lines represent the accumulated inverse Λ_{eff} given by Matthiessen's rule.

dominated by grain boundary scattering at low temperatures (i.e., $T \ll \theta_D$, where θ_D denotes the Debye temperature) and by Umklapp scattering at high temperatures ($T \gg \theta_D$).

Figure 3(a) illustrates the temperature-dependent k_x of nanograined silicon with a constant grain area of 10 000 nm^2 and varying ξ. For $\xi < 1$, k_x decreases with decreasing ξ due to an increase in interfacial density along the heat flux direction, ϕ_x (i.e., more vertical grain boundary lines, also see Table I). These vertical grain boundaries serve as obstacles that scatter phonons, resulting in a shorter Λ_{GB}. Conversely, for $\xi > 1$, an optimal ξ exists that maximizes k_x. A grain structure with $\xi = 16$ yields the highest k_x at a temperature near 150 K. Beyond this transition point, k_x decreases with increasing ξ due to a reduced mean free path between horizontal grain boundary lines that limits the transmission of low-frequency (long wavelength) phonons. This also confirms the inverse trend of Λ_{GB} discussed previously.

To investigate the effect of grain anisotropy on thermal anisotropy, the cross-plane lattice thermal conductivity (k_y) must be evaluated. Given two sets of grain structures with $\xi > 1$ and $\xi < 1$, both incrementing by a power of two, a grain geometry with $\xi = 1/2$ corresponds to a 90° rotation from a grain geometry with $\xi = 2$. Hence, k_x for a grain geometry with $\xi = 1/2$ serves as k_y for a grain geometry with $\xi = 2$. We define the thermal anisotropy ratio (TAR) as the ratio of k_x/k_y to quantify the degree of thermal anisotropy. As shown in Fig. 3(d), the TAR monotonically increases with ξ, even at high temperatures. However, the increase in TAR for high-ξ structures becomes less pronounced at high temperatures, primarily due to the dominance of Umklapp scattering over grain boundary scattering at high temperatures.

To investigate the mechanical behaviors and elastic anisotropy of nanograined silicon, we conducted MD simulations on three anisotropic grain structures. These structures possess the same grain area (a_0^2) or effective grain size (a_0) but have aspect ratios of 2, 1, and 1/2, respectively. Starting with these initial structures, we scaled them to yield structures with varying a_0 and applied uniaxial tension and shear stress to determine the moduli (see supplementary material Note 6 for details on the strain rate and time step). It is worth mentioning that we introduced a small degree of grain heterogeneity to ensure mechanical stability at the grain boundary junctions, but the designed grain heterogeneity has a negligible impact on the moduli due to the weak grain boundary activities observed during micro-elastic deformation. Instead, the moduli are significantly affected by a_0 and ξ.

As illustrated in Figs. 4(d) and 4(h), both the elastic modulus (E) and shear modulus (G) decrease as a_0^2 or a_0 decreases. These rapid reductions can be attributed to an increase in the grain boundary density or the volume percentage of grain boundary atoms. In contrast to

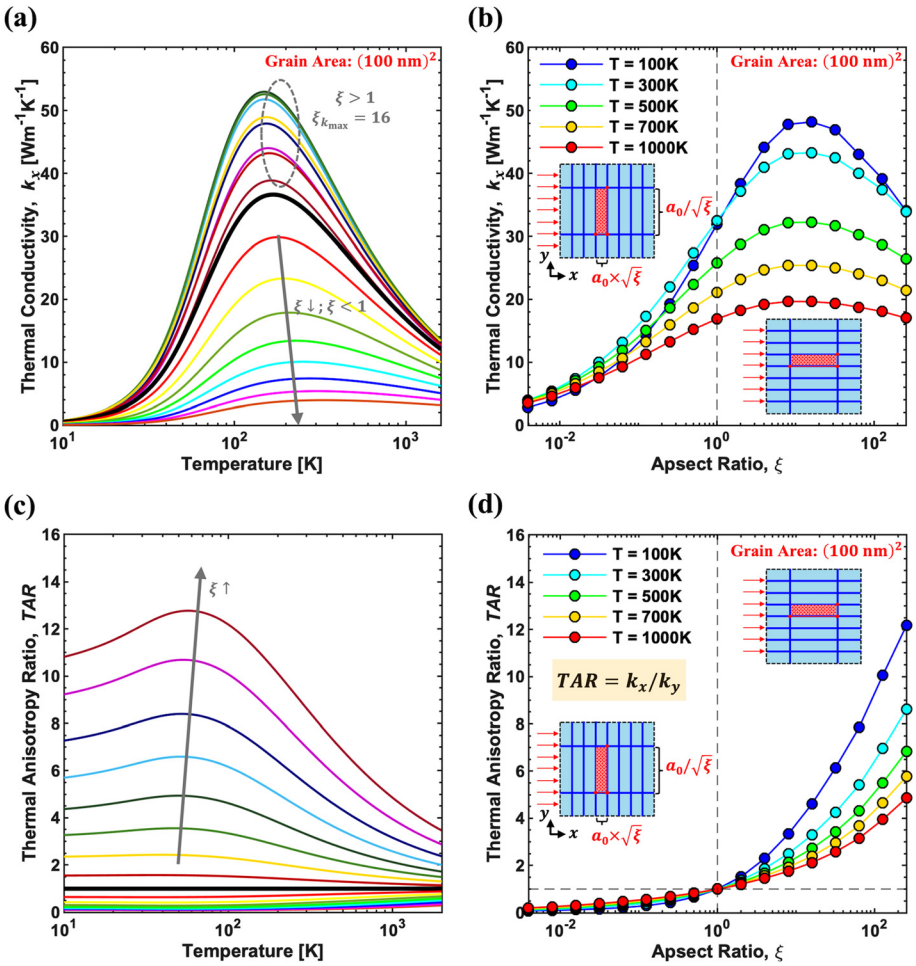

FIG. 3. (a) Temperature-dependent lattice thermal conductivity of nanograined silicon with varying grain aspect ratios. (b) k_x as a function of grain aspect ratio. (c) Thermal anisotropy ratio (TAR) as a function of temperature and (d) grain aspect ratio, respectively.

the regularly packed atoms within grain interiors, grain boundary atoms exhibit disordered arrangements that weaken their interatomic bonding and lead to material softening. Furthermore, we observe a strong dependence of E on ξ. A grain structure with $\xi = 2$ exhibits the highest E across all a_0, while that with $\xi = 1/2$ yields the lowest E. In the elastic regime, when nanograined silicon experiences tension, atoms are purely stretched along the loading direction. The designed grain anisotropy alters the grain boundary distribution along the loading direction, affecting both the stretchability and E. Nevertheless, the fact that the loading direction does not perfectly align with the shear direction diminishes the effect of grain anisotropy on shear deformation. Hence, there is no apparent correlation between G and ξ.

While reducing the grain size effectively decreases the thermal conductivity through boundary scatterings, the effect of lattice softening on the phonon group velocity needs to be addressed when the effective grain size falls below a critical limit. To account for this, we modify the BvK dispersion relation by introducing a lattice softening factor, F_s, into the isotropic approximation,[34]

$$\omega = \frac{2}{\pi} F_s V_{bulk} q_0 \sin\left(\frac{\pi q}{2q_0}\right). \tag{4}$$

Here, F_s is defined as the ratio of the softened speed of sound to the bulk speed of sound (i.e., $F_s = V_{softened}/V_{bulk}$), q is the wavevector, and q_0 is the cutoff wavevector set by the atomic number density. In this study, we determine the average softened speed of sound, using the following expression:[35,51]

$$\frac{3}{V_{softened}^3} = \frac{1}{V_L^3} + \frac{2}{V_T^3}, \tag{5}$$

where $V_L = \sqrt{C_{11}/\rho}$ and $V_T = \sqrt{C_{44}/\rho}$ represent the longitudinal and transverse speeds of sound, respectively. C_{11} and C_{44} are the elements of the elastic matrix, and ρ is the density (see supplementary material Note 7 for more details on the elastic matrix and the derivation of speeds of sound for elastic waves in cubic crystals). The C_{44} element coincides with the shear modulus (G), and C_{11} is the ratio of a uniaxial stress to the corresponding longitudinal strain when the lateral expansion/contraction is impeded. For nanomaterials, which possess large surface ratios, we approximate $V_L \approx \sqrt{E/\rho}$ using the Young's modulus or the elastic modulus (E) because it is effective in quantifying the elastic constants of nanomaterials with free boundary conditions. It is noted that, with the free lateral boundary condition, E has a smaller value than C_{11} due to Poisson's effect, which could result in a

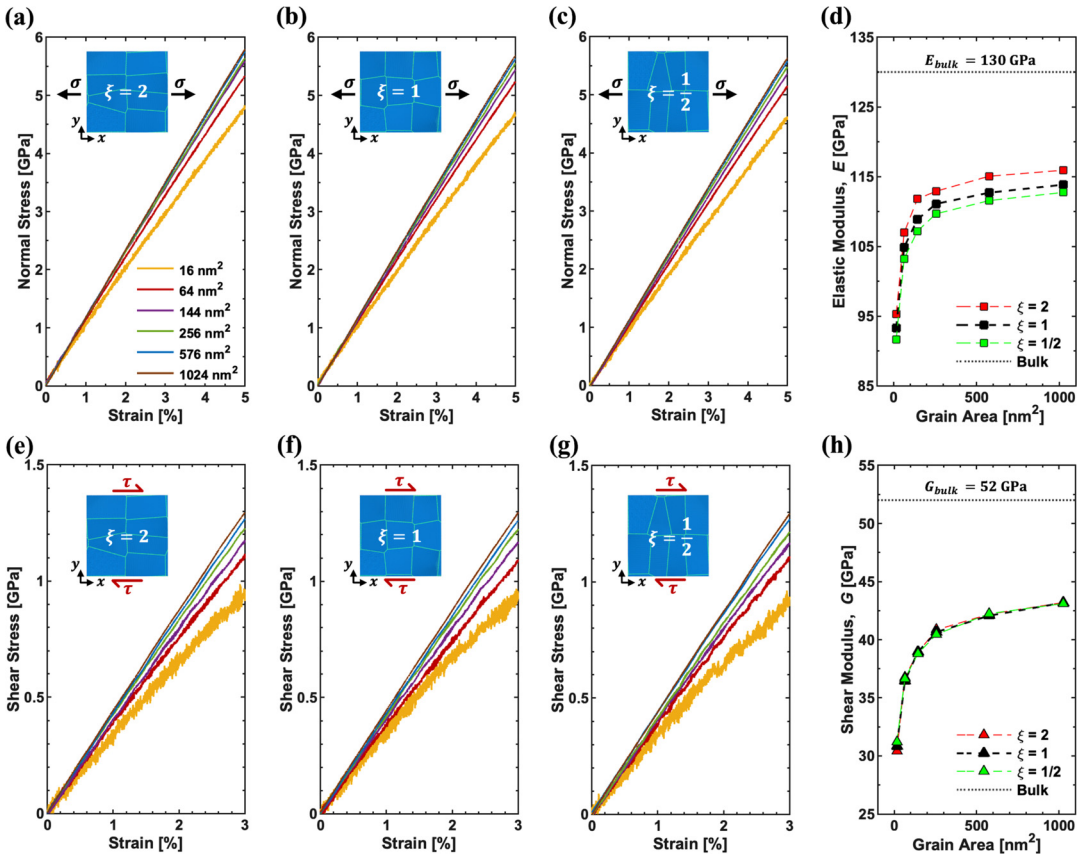

FIG. 4. Tension and shear responses of nanograined silicon. Strain–stress behaviors of nanograined silicon with (a) and (e) $\xi = 2$, (b) and (f) $\xi = 1$, and (c) and (g) $\xi = 1/2$. (d) Elastic modulus and (h) shear modulus as a function of grain size for the corresponding nanograined structures. The dotted lines indicate the reported E and G values for bulk silicon.[50]

TABLE II. Elastic moduli, shear moduli, softened speeds of sound, and lattice softening factors for nanograined silicon with aspect ratios (ξ) of 1, 2, and 1/2 and grain areas (a_0^2) ranging from 16 nm^2 to 1024 nm^2. (We use $\rho = 2328\ \mathrm{kg/m^3}$ for bulk silicon.).

Grain area, a_0^2 (effective grain size, a_0)	16 nm^2 (4 nm)	64 nm^2 (8 nm)	144 nm^2 (12 nm)	256 nm^2 (16 nm)	576 nm^2 (24 nm)	1024 nm^2 (32 nm)
$\xi = 1$						
E (GPa)	93.24	104.87	108.86	111.09	112.69	113.83
G (GPa)	30.83	36.44	38.96	40.66	42.06	43.17
$V_{softened}$ (m/s)	4042	4384	4527	4619	4694	4751
F_s	0.664	0.721	0.744	0.759	0.772	0.781
$\xi = 2$						
E (GPa)	95.27	106.96	111.81	112.89	115.05	115.91
G (GPa)	30.42	36.74	38.92	40.85	42.19	43.19
$V_{softened}$(m/s)	4021	4404	4531	4633	4705	4757
F_s	0.661	0.724	0.745	0.762	0.773	0.782
$\xi = 1/2$						
E (GPa)	91.63	103.22	107.19	109.66	111.56	112.74
G (GPa)	31.20	36.63	38.81	40.46	42.24	43.10
$V_{softened}$(m/s)	4060	4391	4516	4606	4700	4745
F_s	0.667	0.722	0.742	0.757	0.773	0.780

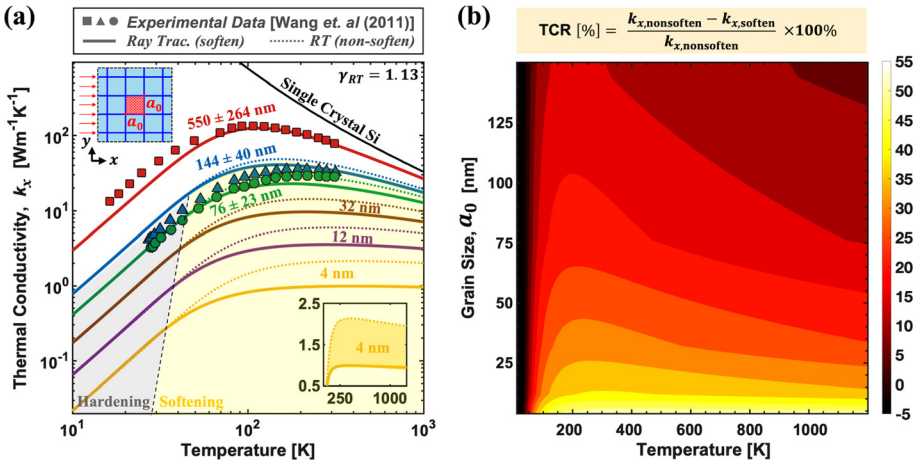

FIG. 5. (a) Temperature-dependent lattice thermal conductivity of nanograined silicon with $\xi = 1$ and varying a_0. The dotted lines show the calculated thermal conductivity using the BvK dispersion relation for bulk silicon. The solid lines represent the size-dependent thermal conductivity accounting for lattice softening and its impact on the phonon group velocity (i.e., using the modified BvK dispersion relation and a softening factor determined by the elastic properties from MD simulations). The scattered data points correspond to the experiential data from Wang *et al.*[1] (b) Contour plot illustrating the percentage of thermal conductivity reduction (TCR) as a function of temperature and grain size.

smaller value for the longitudinal velocity V_L, leading to a reduced lattice softening factor F_s or an overestimation of lattice softening behavior. Table II shows the elastic moduli, shear moduli, softened speeds of sound, and lattice softening factors for the same nanograined structures presented in Fig. 4.

Figure 5(a) shows the temperature-dependent lattice thermal conductivity of nanograined silicon with $\xi = 1$ and varying a_0. As a_0 increases, the solid lines gradually converge toward the dash lines because the elastic properties of nanograined silicon approach those of bulk silicon, rendering the softening effect negligible. Based on the extrapolated data from MD simulations, we determined this critical a_0 to be approximately 125 to 140 nm (see supplementary material Note 8 and Fig. S8). Therefore, for nanograined silicon with an a_0 smaller than 140 nm, it is important to consider lattice softening and its impact on the size-dependent thermal conductivity.

In general, the lattice softening effect has a more pronounced impact on reducing thermal conductivity in materials with smaller grain sizes and at higher temperatures. For instance, nanograined silicon with an a_0 of 4 nm experiences a roughly 50% reduction in k_L at temperatures above 150 K. While lattice softening decreases high-temperature thermal conductivity, it increases low-temperature thermal conductivity. As shown in Fig. 5(b), this increase is less than 5% at temperatures lower than 50 K. This "hardening" effect can potentially be attributed to the competing influences of an increased volumetric heat capacity ($C_v \propto v_g^{-3}$) and a reduced effective mean free path ($\Lambda_{eff} = v_g \tau_{eff} \propto v_g^1$) resulting from a softened group velocity (see supplementary material Note 9 and Fig. S9 for more details).

In summary, controlling the grain size and aspect ratio in nanostructures is crucial for achieving optimal thermal conductivity reduction and thermomechanical anisotropy. Our study of nanograined silicon with varying a_0 and ξ reveals two distinct regimes of thermal transport: (1) anisotropic phonon–grain boundary scattering becomes more prominent at low temperatures, with low-frequency phonons predominantly contributing to the substantial thermal conductivity anisotropy, and (2) lattice softening becomes more appreciable at high temperatures, with high-frequency phonons being responsible for the softening-driven thermal conductivity reduction. The guidelines presented here, harnessing phonon–grain boundary scattering and lattice softening, underscore the importance of microstructure engineering in tailoring the thermomechanical properties of nanomaterials. These findings hold meaningful implications for multifunctional materials in applications such as thermoelectric cooling, power generation, and thermal management.

See the supplementary material for more details on: (1) the phonon/lattice softening effect and its implication on the lattice thermal conductivity; (2) the Boltzmann transport equation (BTE) model for thermal conductivity; (3) the Mote Carlo Ray Tracing framework and algorithm; (4) the convergence and fitting of mean free path for grain boundary scattering; (5) the model validation; (6) molecular dynamics simulations; (7) elastic matrix and elastic waves in cubic crystals; (8) determining the critical grain size for lattice softening; and (9) implications of softened/reduced group velocity on thermal conductivity.

J.C., L.F.-A., and J.L. acknowledge the support provided by the National Science Foundation (Nos. ECCS-1807825 and CMMI-1935371).

AUTHOR DECLARATIONS

Conflict of Interest

The authors have no conflicts to disclose.

Author Contributions

Jiahui Cao: Conceptualization (lead); Data curation (lead); Formal analysis (lead); Investigation (lead); Methodology (lead); Software (lead); Validation (lead); Visualization (lead); Writing – original draft (lead); Writing – review & editing (equal). **Han Wang:** Conceptualization (equal); Data curation (equal); Formal analysis (equal); Investigation (equal); Methodology (equal); Software (equal); Validation (equal); Visualization (equal); Writing – original draft (equal); Writing – review & editing (equal). **Laia Ferrer-Argemi:** Conceptualization (equal); Data curation (equal); Formal analysis (equal); Investigation (equal); Methodology (equal); Software (equal); Validation (equal); Visualization (equal); Writing – review & editing (equal). **Penghui Cao:** Conceptualization (equal); Funding acquisition (equal); Project administration (equal); Resources (equal); Supervision (equal); Validation (equal); Writing – review & editing (equal). **Jaeho**

Lee: Conceptualization (equal); Funding acquisition (lead); Project administration (lead); Resources (lead); Supervision (lead); Validation (equal); Writing – review & editing (equal).

DATA AVAILABILITY

The data that support the findings of this study are available from the corresponding author upon reasonable request.

REFERENCES

[1]Z. Wang, J. E. Alaniz, W. Jang, J. E. Garay, and C. Dames, "Thermal conductivity of nanocrystalline silicon: Importance of grain size and frequency-dependent mean free paths," Nano Lett. **11**(6), 2206–2213 (2011).

[2]T. Hori, J. Shiomi, and C. Dames, "Effective phonon mean free path in polycrystalline nanostructures," Appl. Phys. Lett. **106**(17), 171901 (2015).

[3]S. Alaie, D. F. Goettler, M. Su, Z. C. Leseman, C. M. Reinke, and I. El-Kady, "Thermal transport in phononic crystals and the observation of coherent phonon scattering at room temperature," Nat. Commun. **6**, 7228 (2015).

[4]P. E. Hopkins, C. M. Reinke, M. F. Su, R. H. Olsson, E. A. Shaner, Z. C. Leseman, J. R. Serrano, L. M. Phinney, and I. El-Kady, "Reduction in the thermal conductivity of single crystalline silicon by phononic crystal patterning," Nano Lett. **11**(1), 107–112 (2011).

[5]J. Lee, J. Lim, and P. Yang, "Ballistic phonon transport in holey silicon," Nano Lett. **15**(5), 3273–3279 (2015).

[6]W. Park, J. Sohn, G. Romano, T. Kodama, A. Sood, J. S. Katz, B. S. Y. Kim, H. So, E. C. Ahn, M. Asheghi, A. M. Kolpak, and K. E. Goodson, "Impact of thermally dead volume on phonon conduction along silicon nanoladders," Nanoscale **10**(23), 11117–11122 (2018).

[7]D. Li, Y. Wu, P. Kim, L. Shi, P. Yang, and A. Majumdar, "Thermal conductivity of individual silicon nanowires," Appl. Phys. Lett. **83**(14), 2934–2936 (2003).

[8]A. I. Hochbaum, R. Chen, R. D. Delgado, W. Liang, E. C. Garnett, M. Najarian, A. Majumdar, and P. Yang, "Enhanced thermoelectric performance of rough silicon nanowires," Nature **451**(7175), 163–167 (2008).

[9]A. I. Boukai, Y. Bunimovich, J. Tahir-Kheli, J. K. Yu, W. A. Goddard, and J. R. Heath, "Silicon nanowires as efficient thermoelectric materials," Nature **451**(7175), 168–171 (2008).

[10]J. K. Yu, S. Mitrovic, D. Tham, J. Varghese, and J. R. Heath, "Reduction of thermal conductivity in phononic nanomesh structures," Nat. Nanotechnol. **5**(10), 718–721 (2010).

[11]J. Lee, W. Lee, G. Wehmeyer, S. Dhuey, D. L. Olynick, S. Cabrini, C. Dames, J. J. Urban, and P. Yang, "Investigation of phonon coherence and backscattering using silicon nanomeshes," Nat. Commun. **8**, 14054 (2017).

[12]L. Yang, Y. Zhao, Q. Zhang, J. Yang, and D. Li, "Thermal transport through fishbone silicon nanoribbons: Unraveling the role of Sharvin resistance," Nanoscale **11**(17), 8196–8203 (2019).

[13]M. S. Jeng, R. Yang, D. Song, and G. Chen, "Modeling the thermal conductivity and phonon transport in nanoparticle composites using Monte Carlo simulation," J Heat Transfer **130**(4), 042410 (2008).

[14]S. Mazumder and A. Majumdar, "Monte Carlo study of phonon transport in solid thin films including dispersion and polarization," J. Heat Transfer **123**(4), 749–759 (2001).

[15]D. Lacroix, K. Joulain, and D. Lemonnier, "Monte Carlo transient phonon transport in silicon and germanium at nanoscales," Phys. Rev. B **72**(6), 064305 (2005).

[16]J. Ma, B. R. Parajuli, M. G. Ghossoub, A. Mihi, J. Sadhu, P. V. Braun, and S. Sinha, "Coherent phonon-grain boundary scattering in silicon inverse opals," Nano Lett. **13**(2), 618–624 (2013).

[17]C. Kimmer, S. Aubry, A. Skye, and P. K. Schelling, "Scattering of phonons from a high-energy grain boundary in silicon: Dependence on angle of incidence," Phys. Rev. B **75**(14), 144105 (2007).

[18]C. Hua, X. Chen, N. K. Ravichandran, and A. J. Minnich, "Experimental metrology to obtain thermal phonon transmission coefficients at solid interfaces," Phys. Rev. B **95**(20), 205423 (2017).

[19]Q. Hao, G. Zhu, G. Joshi, X. Wang, A. Minnich, Z. Ren, and G. Chen, "Theoretical studies on the thermoelectric figure of merit of nanograined bulk silicon," Appl. Phys. Lett. **97**(6), 063109 (2010).

[20]C. Hua and A. J. Minnich, "Importance of frequency-dependent grain boundary scattering in nanocrystalline silicon and silicon-germanium thermoelectrics," Semicond. Sci. Technol. **29**(12), 124004 (2014).

[21]D. Chakraborty, S. Foster, and N. Neophytou, "Monte Carlo phonon transport simulations in hierarchically disordered silicon nanostructures," Phys. Rev. B **98**(11), 115435 (2018).

[22]L. Yang and A. J. Minnich, "Thermal transport in nanocrystalline Si and SiGe by *ab initio* based Monte Carlo simulation," Sci. Rep. **7**, 44254 (2017).

[23]H. Yang, J. H. Bahk, T. Day, A. M. S. Mohammed, G. J. Snyder, A. Shakouri, and Y. Wu, "Enhanced thermoelectric properties in bulk nanowire heterostructure-based nanocomposites through minority carrier blocking," Nano Lett. **15**(2), 1349–1355 (2015).

[24]H. Fang and Y. Wu, "Telluride nanowire and nanowire heterostructure-based thermoelectric energy harvesting," J. Mater. Chem. A **2**(17), 6004–6014 (2014).

[25]E. O. Hall, "The deformation and ageing of mild steel: III Discussion of results," Proc. Phys. Soc. B **64**(9), 747–753 (1951).

[26]C. V. Di Leo and J. J. Rimoli, "New perspectives on the grain-size dependent yield strength of polycrystalline metals," Scr. Mater. **166**, 149–153 (2019).

[27]N. Tsuji, Y. Ito, Y. Saito, and Y. Minamino, "Strength and ductility of ultrafine grained aluminum and iron produced by ARB and annealing," Scr. Mater. **47**(12), 893–899 (2002).

[28]J. Schiøtz, F. D. Di Tolla, and K. W. Jacobsen, "Softening of nanocrystalline metals at very small grain sizes," Nature **391**(6667), 561–563 (1998).

[29]N. Hansen, "Hall-petch relation and boundary strengthening," Scr. Mater. **51**(8), 801–806 (2004).

[30]O. A. Ageev, E. Y. Gusev, J. Y. Jityaeva, M. V. Ilina, and A. V. Bykov, "Grain size and doping effect on structure and electromechanical properties of polycrystalline silicon for MEMS applications," J. Phys.: Conf. Ser. **741**(1), 012001 (2016).

[31]V. I. Ivashchenko, P. E. A. Turchi, and V. I. Shevchenko, "Simulations of the mechanical properties of crystalline, nanocrystalline, and amorphous SiC and Si," Phys. Rev. B **75**(8), 085209 (2007).

[32]W. N. Sharpe, K. T. Turner, and R. L. Edwards, "Tensile testing of polysilicon," Exp. Mech. **39**(3), 162–170 (1999).

[33]S. Goel, A. Kovalchenko, A. Stukowski, and G. Cross, "Influence of microstructure on the cutting behaviour of silicon," Acta Mater. **105**, 464–478 (2016).

[34]M. D. Gerboth and D. G. Walker, "Effects of acoustic softening on thermal conductivity beyond group velocity," J. Appl. Phys. **127**(20), 204302 (2020).

[35]R. Hanus, M. T. Agne, A. J. E. Rettie, Z. Chen, G. Tan, D. Y. Chung, M. G. Kanatzidis, Y. Pei, P. W. Voorhees, and G. J. Snyder, "Lattice softening significantly reduces thermal conductivity and leads to high thermoelectric efficiency," Adv. Mater. **31**(21), 1900108 (2019).

[36]J. F. Li, W. S. Liu, L. D. Zhao, and M. Zhou, "High-performance nanostructured thermoelectric materials," NPG Asia Mater. **2**(4), 152–158 (2010).

[37]M. Zhang, K. Sun, and L. Fang, "Influence of grain boundary activites on elastic and plastic deformation of nanocrystalline Cu as studied by phase filed and atomistic simulaiton," Int. J. Mech. Sci. **187**, 105911 (2020).

[38]C. Dames and G. Chen, "Theoretical phonon thermal conductivity of Si/Ge superlattice nanowires," J. Appl. Phys. **95**(2), 682–693 (2004).

[39]F. Yang and C. Dames, "Mean free path spectra as a tool to understand thermal conductivity in bulk and nanostructures," Phys. Rev. B **87**(3), 035437 (2013).

[40]M. Asen-Palmer, K. Bartkowski, E. Gmelin, M. Cardona, A. P. Zhernov, A. V. Inyushkin, A. Taldenkov, V. I. Ozhogin, K. M. Itoh, and E. E. Haller, "Thermal conductivity of germanium crystals with different isotopic compositions," Phys. Rev. B **56**(15), 9431–9447 (1997).

[41]C. J. Glassbrenner and G. A. Slack, "Thermal conductivity of silicon and germanium from 3 K to the melting point," Phys. Rev. **134**(4), A1058 (1964).

[42]Z. Yu, L. Ferrer-Argemi, and J. Lee, "Investigation of thermal conduction in symmetric and asymmetric nanoporous structures," J. Appl. Phys. **122**(24), 244305 (2017).

[43]L. Ferrer-Argemi, Z. Yu, and J. Lee, "Effects of metal silicide inclusion interface and shape on thermal transport in silicon nanocomposites," J. Appl. Phys. **126**(3), 035106 (2019).

[44]M. Morita, T. Ohmi, E. Hasegawa, M. Kawakami, and M. Ohwada, "Growth of native oxide on a silicon surface," J. Appl. Phys. **68**(3), 1272–1281 (1990).

[45]X. Li and R. Yang, "Effect of lattice mismatch on phonon transmission and interface thermal conductance across dissimilar material interfaces," Phys. Rev. B **86**(5), 054305 (2012).

[46]Z. Tian, K. Esfarjani, and G. Chen, "Enhancing phonon transmission across a Si/Ge interface by atomic roughness: First-principles study with the Green's function method," Phys. Rev. B **86**(23), 235304 (2012).
[47]B. Li, C. Zhang, B. Jiang, W. Han, and Z. Lin, "Flow-enabled self-assembly of large-scale aligned nanowires," Angew. Chem. **127**(14), 4324–4328 (2015).
[48]C. M. Hangarter, Y. Rheem, B. Yoo, E. H. Yang, and N. V. Myung, "Hierarchical magnetic assembly of nanowires," Nanotechnology **18**(20), 205305 (2007).
[49]J. Yao, H. Yan, and C. M. Lieber, "A nanoscale combing technique for the large-scale assembly of highly aligned nanowires," Nat. Nanotechnol. **8**(5), 329–335 (2013).
[50]M. A. Hopcroft, W. D. Nix, and T. W. Kenny, "What is the Young's modulus of silicon?," J. Microelectromech. Syst. **19**(2), 229–238 (2010).
[51]O. L. Anderson, "A simplified method for calculating the Debye temperature from elastic constants," J. Phys. Chem. Solids **24**, 909–917 (1963).